Editors' Suggestion

Full-Duplex Nonreciprocal Beam Steering by Time-Modulated Phase-Gradient Metasurfaces

Sajjad Taravati* and George V. Eleftheriades

The Edward S. Rogers Sr. Department of Electrical and Computer Engineering, University of Toronto, Toronto, Ontario M5S 3H7, Canada

(Received 13 December 2019; revised 21 January 2020; accepted 1 June 2020; published 9 July 2020)

We present the concept, theoretical model, and experimental implementation of a full-duplex nonreciprocal-beam-steering transmissive phase-gradient metasurface. Such a metasurface is realized by exploiting the unique properties of the frequency-phase transition in time-modulated twin unit cells. The metasurface may be placed on top of a source antenna to transform the radiation pattern of the source antenna, and introduce different radiation patterns for the transmit and receive states. In contrast to the recently proposed applications of time modulation, here the incident and transmitted waves share the same frequency. The metasurface is endowed with directive, diverse, and asymmetric transmission and reception radiation beams, and tunable beam shapes. Furthermore, these beams can be steered by simply changing the modulation phase. The proposed twin unit cells inherently suppress undesired time harmonics, leading to a high conversion efficiency, which is of paramount importance for practical applications such as point-to-point full-duplex communications.

DOI: 10.1103/PhysRevApplied.14.014027

I. INTRODUCTION

The ever increasing progress in wireless telecommunication systems demands a class of compact structures, called metasurfaces, for wave engineering and controlling the electromagnetic wave radiation [1–5]. Even though conventional reciprocal and static metasurfaces are capable of providing quite useful operations, nonreciprocity and time modulation can bring metasurfaces to a different level, introducing peculiar and unique wave-engineering functionalities not seen in conventional metamaterials and metasurfaces [2,6–8]. Conventional metamaterials and metasurfaces are resonator-based passive linear time-invariant structures that are limited by Lorentz reciprocity theorem [9]. Hence, they are lossy and cannot introduce a range of useful functionalities such as nonreciprocal wave transmission, unidirectional or bidirectional wave amplification, and frequency generation. To overcome this issue, a surge of study on dynamic and nonreciprocal metamaterial and metasurface technologies has been commenced [10–13].

Nonreciprocity based on time modulation represents a powerful tool for advanced wave engineering and extraordinary control over electromagnetic waves [7,13–21]. Recently, there has been a deep investigation on wave propagation and scattering in time-periodic [8,22–25] and space-time-periodic [17,19,26–31] media. Time modulation represents a thrilling topic thanks to the complexity and rich physics of the problem, as well as the diverse and exciting practical applications of time modulation. Time modulation has been recently used for the realization of isolators and nonreciprocal platforms [26,32–39], circulators [40,41], metasurfaces [1,3,7,42–44], frequency converters [5,45], mixer duplexer antennas [46], antennas [6,47–53], unidirectional beam splitters [20], nonreciprocal filters [54,55], and impedance matching structures [56]. Other recently reported outstanding and unique properties and applications of space-time-periodic media include anomalous topological edge states in space-time photonic crystal [28], Fresnel drag [57], signal-coding metagratings [58], and antenna mixer amplifiers [59].

Previously reported time-modulated metasurfaces suffer from an undesired frequency alteration in the spectrum of the incident wave. Such a frequency change is usually undesired as the frequency of the up- or down-converted wave is very close to the incident wave and cannot be represented as an effective mixing functionality. In addition, the converted wave is usually accompanied by an infinite number of higher-order time harmonics, which leads to a crowded frequency spectrum, poor conversion efficiency, and may result in intermodulation interference. Another important point is that most of the previously reported time-modulated metasurfaces are reflective structures [1,3,6,42,43], which may not be as practical as transmissive metasurfaces.

This study presents the concept, theoretical model, and experimental implications of full-duplex nonreciprocal-beam-steering transmissive phase-gradient metasurfaces.

*sajjad.taravati@utoronto.ca

Such metasurfaces are realized by exploiting the unique properties of the asymmetric frequency-phase electromagnetic transitions in time-modulated particles. It is shown that when the refractive index of structures is time modulated, the incident wave experiences interband electromagnetic transitions between electromagnetic states due to temporal and spatial frequency shifts [13,38,60,61], in analogy to electronic transitions in semiconductors.

Such metasurfaces may be placed on top of a source antenna, transforming their radiation pattern and providing different radiation patterns for the transmit and receive states. Such metasurfaces are composed of an array of twin time-modulated unit cells, each of which functioning four major operations, i.e., wave reception, nonreciprocal phase shift for nonreciprocal beam steering, filtering out of unwanted temporal harmonics, and wave radiation.

The contribution of this work is as follows. We propose a metasurface that can be used for multifunctionality purposes, i.e., different radiation patterns (e.g., different half-power beamwidths and different angle of radiation, as well as, different signal amplifications) for transmission and reception, nonreciprocal beam steering and beam shaping. Such a metasurface provides highly directive and tunable beams for point-to-point full-duplex telecommunications. In addition, from the physical point of view, this study presents a time-modulated antenna metasurface platform, where the incident and transmitted waves share the same temporal frequency, different than other previously reported time-modulated radiating metasurfaces. We propose the concept of twin time-modulated unit cells, and take advantage of the physical phenomena that occur in such structures. Specifically, the nonreciprocal phase shift in a round-trip electromagnetic transition in periodic time-modulated media with zero frequency alteration, the transmissive reception and reradiation of the electromagnetic waves, as well as the filtering of undesired temporal harmonics. The proposed twin time-modulated unit cells inherently prohibits the excitation of undesired time harmonics, leading to a high conversion efficiency, which is of paramount importance for practical applications such as, for instance, point-to-point full-duplex telecommunications.

Firstly, we present the concept of the full-duplex nonreciprocal-beam-steering transmissive metasurface. Subsequently, we present the theoretical, physical, and practical implications of nonreciprocal phase shift in twin time-modulated unit cells. We next propose the implementation scenario for the practical realization of a full-Duplex nonreciprocal-beam-steering transmissive metasurface induced by phase-gradient time-modulated twin unit cells. Subsequently, we present full-wave simulation, as well as experimental results for symmetric and asymmetric radiation beams at different angles of radiation.

II. CONCEPT OF NONRECIPROCAL RADIATION BEAM

Figure 1 illustrates the functionality of the nonreciprocal radiation beam from a gradient metasurface for efficient full-duplex point-to-point telecommunications. In the transmission state (TX), the wave is launched from the source antenna traveling along the $+z$ direction, passes through the metasurface from region 1 to region 2 and radiates at an angle $\theta_{2,\mathrm{TX}}$. In contrast, in the receive state (RX), the metasurface presents the maximum transmission from region 2 to region 1 for the incoming wave at angle $\theta_{2,\mathrm{RX}}$. Therefore, for a given radiation angle θ_0, the metasurface is nonreciprocal, and may be represented by asymmetric and nonreciprocal radiation beams, as

$$F_{\mathrm{TX}}(\theta) \neq F_{\mathrm{RX}}(\theta), \tag{1}$$

where $F_{\mathrm{TX}}(\theta) = E_{\theta,\mathrm{TX}}/E_{\theta,\mathrm{TX}}(\mathrm{max})$ and $F_{\mathrm{RX}}(\theta) = E_{\theta,\mathrm{RX}}/E_{\theta,\mathrm{RX}}(\mathrm{max})$.

To realize the full-duplex nonreciprocal-beam-steering radome in Fig. 1, we consider a transmissive metasurface formed by an array of unit cells. Figure 2 depicts

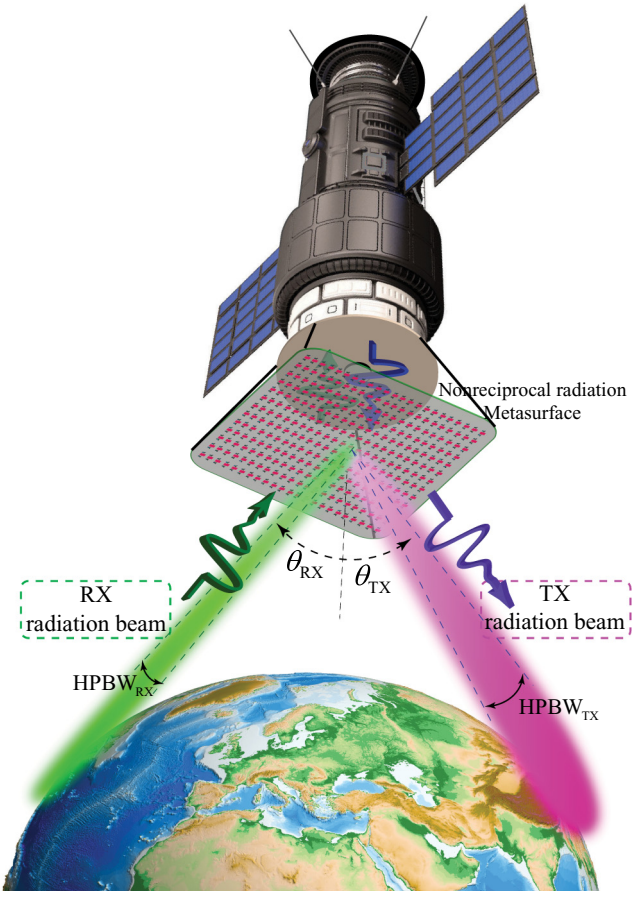

FIG. 1. Full-duplex nonreciprocal radiation beam yielding highly directive reception and transmission radiation beams for efficient full-duplex point-to-point telecommunications.

the structure of the metasurface sandwiched between two semi-infinite regions, i.e., region 1 and region 2. Qualitative radiation beams for the transmission and reception states at the two sides of the metasurface are sketched to show the operation principle of the structure. In the transmission state, a plane wave with frequency ω_i impinges on the metasurface from the bottom left side with an angle of incidence $\theta_{1,\mathrm{TX}}$. The outgoing wave at $\theta_{2,\mathrm{TX}}$ acquires a discrete phase profile $\phi(x)$,

$$\phi(md) = \phi_m, \tag{2}$$

where m is the modulation phase at the mth unit cell and d is the spacing between each of the two adjacent unit cells. However, in the transmission state, considering the scheme in Fig. 2, a plane wave with frequency ω_i impinges on the metasurface from the top right side with an angle of incidence $\theta_{2,\mathrm{RX}}$. In contrast to the transmission state, and due to the conservation of momentum, the outgoing wave at $\theta_{1,\mathrm{RX}}$ acquires a discrete phase profile $\phi(x)$, where

$$-\phi(md) = -\phi_m. \tag{3}$$

Assuming a constant gradient phase shift along the metasurface, the generalized Snell law of refraction yields

$$\frac{\partial \phi_{\mathrm{TX}}}{\partial x} = k_2 \sin(\theta_{2,\mathrm{TX}}) - k_1 \sin(\theta_{1,\mathrm{TX}}), \tag{4}$$

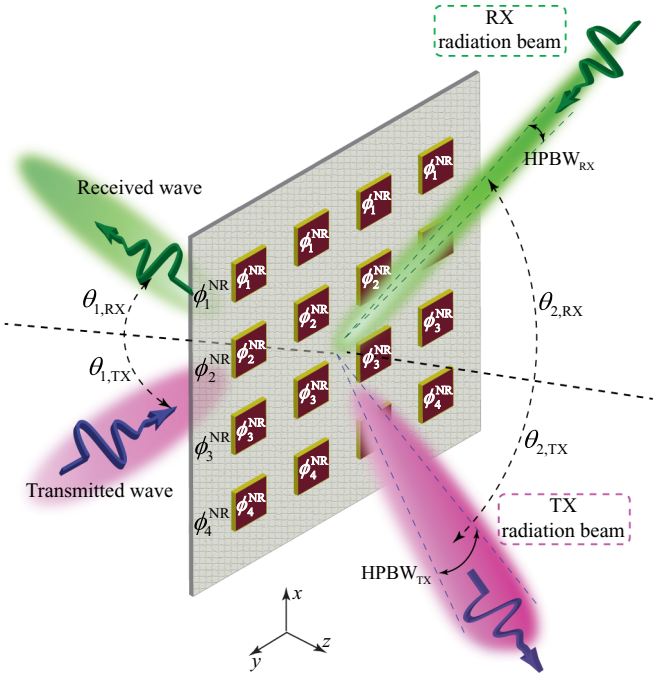

FIG. 2. Schematic representation of the gradient metasurface formed by nonreciprocal phase-shift unit cells.

for the transmission state, and

$$\frac{\partial \phi_{\mathrm{RX}}}{\partial x} = k_2 \sin(\theta_{2,\mathrm{RX}}) - k_1 \sin(\theta_{1,\mathrm{RX}}), \tag{5}$$

for the reception state. Here, k_1 and k_2 are the wave numbers in region 1 and region 2, respectively. Considering a constant phase gradient $\partial\phi/\partial x$, the outgoing wave acquires anomalous refraction with respect to the incident wave, whereas a spatially variant gradient, i.e., $\partial\phi/\partial x$, leads to arbitrary radiation beams, which enables beam-forming and advanced beam-steering purposes.

III. THEORETICAL IMPLICATIONS

A. Theory of nonreciprocal phase shift based on time modulation

Figure 3 sketches the wave propagation and transmission in a periodic time-modulated medium, characterized with a periodic time-dependent permittivity, as

$$\epsilon(t) = \epsilon_{\mathrm{av}} + \delta_\epsilon \cos(\Omega t + \phi_1), \tag{6}$$

where ϵ_{av} is the average permittivity of the background medium, δ_ϵ is the modulation amplitude, Ω denotes the modulation frequency, and ϕ_1 represents the modulation phase. The right plot in Fig. 3 shows a qualitative dispersion diagram of such a time-modulated periodic medium and electromagnetic transitions between two supported resonant frequencies, ω_i and $\omega_i + \Omega$.

The electric field inside the medium is defined based on the superposition of two supported space-time harmonic fields, i.e.,

$$E_s(x,z,t) = a_A(z)e^{-i(k_A z - \omega_i t)} + a_B(z)e^{-i[k_B z - (\omega_i + \Omega)t]}. \tag{7}$$

We consider $\Omega \ll \omega_i$. The corresponding wave equation reads $c^2\partial^2\mathbf{E}/\partial z^2 = \partial^2[\epsilon_{\mathrm{eq}}(t)\mathbf{E}]/\partial t^2$. Inserting the electric

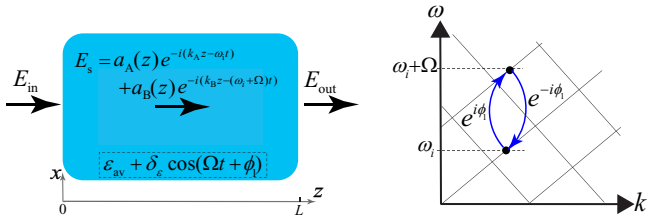

FIG. 3. A time-modulated unit cell with permittivity in Eq. (6). The dispersion diagram demonstrates the general concept of nonreciprocal phase shift based on frequency-phase electromagnetic transitions in a time-modulated unit cell supporting two resonant frequencies, ω_i and $\omega_i + \Omega$, and phase shift ϕ_1.

field in Eq. (7) into the wave equation results in

$$\left(\frac{\partial^2}{\partial z^2}\right)\left\{a_A(z)e^{-i[k_Az-\omega_it)}+a_B(z)e^{-i(k_Az-(\omega_i+\Omega)t]}\right\}$$
$$=\frac{1}{c^2}\frac{\partial^2}{\partial t^2}\left(\left[\epsilon_{\rm av}+\frac{\delta}{2}e^{i(\Omega t+\phi_1)}+\frac{\delta}{2}e^{-i(\Omega t+\phi_1)}\right]\right.$$
$$\left.\times\left\{a_A(z)e^{-i(k_Az-\omega_it)}+a_B(z)e^{-i[k_Az-(\omega_i+\Omega)t]}\right\}\right), \quad (8)$$

and applying the space and time derivatives, while using a slowly varying envelope approximation, multiply both sides with $e^{i(k_Az-\omega_it)}$, which gives

$$\left[k_A^2a_A(z)-2ik_A\frac{\partial a_A(z)}{\partial z}\right]+\left[k_A^2a_B(z)-2i(k_A)\frac{\partial a_B(z)}{\partial z}\right]e^{i\Omega t}$$
$$=\frac{1}{c^2}\left\{\left[\omega_i^2\epsilon_{\rm av}+(\omega_i+\Omega)^2\frac{\delta}{2}e^{i(\Omega t+\phi_1)}\right.\right.$$
$$\left.+(\omega_i-\Omega)^2\frac{\delta}{2}e^{-i(\Omega t+\phi_1)}\right]a_A(z)$$
$$+\left[\omega_i^2\epsilon_{\rm av}+(\omega_i+2\Omega)^2\frac{\delta}{2}e^{i(\Omega t+\phi_1)}\right.$$
$$\left.\left.+\omega_i^2\frac{\delta}{2}e^{-i(\Omega t+\phi_1)}\right]a_B(z)e^{i\Omega t}\right\}, \quad (9)$$

and next, applying $\int_0^{2\pi/\Omega}dt$ to both sides gives

$$\frac{da_A(z)}{dz}=\frac{ik_0^2\delta}{4k_A}e^{-i\phi_1}a_B(z), \quad (10a)$$

where $k_0=(\omega_i+\Omega)/c^2$. Following the same procedure, we next multiply both sides with $e^{-i\Omega t}$, and applying $\int_0^{2\pi/\Omega}dt$ in both sides of the resultant, and applying $\int_0^{2\pi/\Omega}dt$ to both sides of Eq. (9) yields

$$\frac{da_B(z)}{dz}=\frac{ik_0^2\delta}{4k_A}e^{i\phi_1}a_A(z). \quad (10b)$$

Equations (10a) and (10b) represent the coupled-wave equation of the periodic time-modulated medium in Fig. 3.

1. Application of boundary conditions

(i) Considering incidence of a wave with frequency ω_i (up-conversion corresponding to the left arrow in the dispersion diagram in the right side of Fig. 3), i.e., $E_{\rm in}=E_s(z=0)=E_0e^{i\omega_it}$, gives $a_A(z)=E_0\cos(\delta k_1z/4)$, and $a_B(z)=iE_0\sin(\delta k_1z/4)\,e^{i\phi_1}$. Considering the coherence length of $L_c=2\pi k_1/\delta$, $a_A(z=L_c)=0$ and $a_B(z=L_c)=iE_0e^{i\phi_1}$, and

$$E_{\rm out,up\text{-}c}=iE_0e^{-i[k_Bz-(\omega_i+\Omega)t]}e^{i\phi_1}. \quad (11)$$

(ii) Considering incidence of a wave with frequency $\omega_i+\Omega$ (down-conversion corresponding to the right arrow in the dispersion diagram in the right side of Fig. 3), i.e., $E_{\rm in}=E_s(z=0)=E_0e^{i(\omega_i+\Omega)t}$, gives $a_A(z)=iE_0\sin(\delta k_0z/4)\,e^{-i\phi_1}$, and $a_B(z)=E_0\cos(\delta k_0z/4)$. Considering the coherency length of $L_c=2\pi k_0/\delta$, $a_B(z=L_c)=0$ and $a_A(z=L_c)=iE_0e^{-i\phi_1}$, and

$$E_{\rm out,down\text{-}c}=iE_0e^{-i(k_Az-\omega_it)}e^{-i\phi_1}. \quad (12)$$

Equation (11) shows that in the up-conversion electromagnetic transition, i.e., transition from frequency ω_i to $\omega_i+\Omega$, the transmitted up-converted wave acquires the modulation phase shift of ϕ_1. In contrast, Eq. (12) shows that in the down-conversion electromagnetic transition, i.e., the transition from frequency $\omega_i+\Omega$ to ω_i, the wave acquires a negative phase shift, i.e., $-\phi_1$. This shows that the time-modulated medium, with the permittivity in Eq. (6), introduces a nonreciprocal phase shift.

B. Frequency-invariant nonreciprocal radiating phase shifter

In the previous section, we show that a nonreciprocal phase shift may be achieved by taking advantage of electromagnetic transitions in a time-modulated unit cell. However, such a nonreciprocal phase shift is accompanied with a frequency transition, which may not be always desired. Here, we propose a structure that provides a nonreciprocal phase shift without frequency alteration. Figures 4(a) and 4(b) demonstrate the operation principle of the frequency-invariant nonreciprocal radiating phase shifter formed by twin time-modulated unit cells. Figure 4(a) shows a qualitative dispersion diagram of the structure for forward (green arrows) and backward (blue arrows) wave incidences, showing the general concept of the nonreciprocal phase shifting based on electromagnetic transitions in a time-modulated unit cell supporting two resonant frequencies, ω_i and $\omega_i+\Omega$.

In the up-conversion, i.e., the electromagnetic transition from ω_i to $\omega_i+\Omega$, a phase shift of ϕ is achieved, whereas in the down-conversion, that is, the electromagnetic transition from $\omega_i+\Omega$ to ω_i, a phase shift of $-\phi$ is introduced by the time modulation.

The structure of the twin time-modulated unit cells is formed by four resonators, with electric permitivitties

$$\epsilon_1(t)=\epsilon_1+\delta_1\cos(\Omega t+\phi_1), \quad (13a)$$
$$\epsilon_1'(t)=\epsilon_1'+\delta_1'\cos(\Omega t+\phi_1+\pi), \quad (13b)$$
$$\epsilon_2(t)=\epsilon_2+\delta_2\cos(\Omega t+\phi_2), \quad (13c)$$
$$\epsilon_2'(t)=\epsilon_2'+\delta_2'\cos(\Omega t+\phi_2+\pi). \quad (13d)$$

In Fig. 4(b), R_r and R_r' represent the radiation resistances of the first and second unit cells, and K and K' denote the coupling between the arms of the first and second unit cells, whereas K_m is the coupling between the two unit cells.

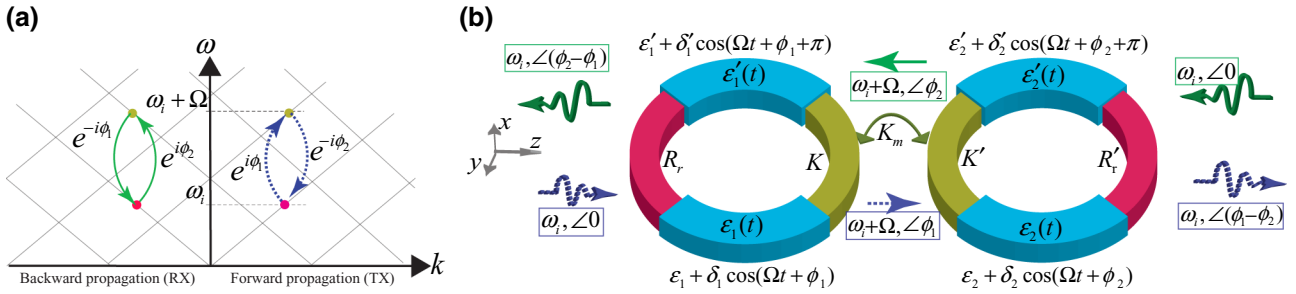

FIG. 4. Nonreciprocal phase-shifted radiation based on electromagnetic transitions in time-modulated media. (a) Dispersion diagram demonstrating nonreciprocal phase shift based on electromagnetic transitions in two time-modulated unit cells supporting two resonant frequencies, ω_i and $\omega_i + \Omega$, and two phase shifts ϕ_1 and ϕ_2. (b) Twin time-modulated radiating unit cells introducing nonreciprocal phase shift for the radiated waves.

In the forward incidence (left to right), the first time-modulated unit cell, characterized with permitivitties $\epsilon_1(t)$ and $\epsilon_1'(t)$, provides a frequency-phase transition from $(\omega_i, 0)$ to $(\omega_i + \Omega, \phi_1)$. Then, the second time-modulated unit cell, characterized with permitivitties $\epsilon_2(t)$ and $\epsilon_2'(t)$, introduces a frequency-phase transition from $(\omega_i + \Omega, \phi_1)$ to $(\omega_i, \phi_1 - \phi_2)$. In contrast, in the backward incidence (right to left), the second time-modulated unit cell, characterized with permitivitties $\epsilon_2(t)$ and $\epsilon_2'(t)$, provides frequency-phase transition from $(\omega_i, 0)$ to $(\omega_i + \Omega, \phi_2)$, and then, the first time-modulated unit cell, characterized with permitivitties $\epsilon_1(t)$ and $\epsilon_1'(t)$, provides frequency-phase transition $(\omega_i + \Omega, \phi_2)$ to $(\omega_i, \phi_2 - \phi_1)$. As a result, no frequency alteration occurs for both forward and backward transmitted waves, whereas a nonreciprocal phase shift is achieved, i.e., the backward transmitted wave acquires the phase shift of $\phi_2 - \phi_1$ which is opposite to that of the forward transmitted wave phase $\phi_1 - \phi_2$.

IV. RESULTS

A. Suppression of unwanted time harmonics

Figure 5 demonstrates the structure of the twin time-modulated unit cells, and the wave scattering and interference inside it, for forward and backward incidences. Since the time-modulated unit cells are periodically modulated in time, the voltage at the two arms of the twin structure may be decomposed to Bloch-Floquet temporal harmonics, such that

$$V(t) = e^{-i\omega_0 t} \sum_{n=-\infty}^{\infty} V_n e^{-in(\Omega t + \phi_1)}, \tag{14a}$$

represents the voltage at the upper arm, and

$$V'(t) = e^{-i\omega_0 t} \sum_{n=-\infty}^{\infty} V_n e^{-in(\Omega t + \phi_1 + \pi)} \tag{14b}$$

represents the voltage at the lower arm of the twin unit cells. Here, $\omega_{-1} = \omega_i$ and $\omega_0 = \omega_i + \Omega$.

It may be seen from Eq. (14) and Fig. 5 that all odd-time harmonics at the two arms of the twin structure are 180° out of phase, whereas even-time harmonics are all in phase. Hence, we apply an interconnector between the two arms of the twin structure with the length of $\lambda_{-1} \simeq \lambda_0$. Considering the 0 and 180° phase shift, respectively, between the even and odd harmonics, the middle interconnector represents an *open circuit* for even-time harmonics and a *short circuit* for odd harmonics. Thereby, as shown in the top figure (forward incidence) of Fig. 5,

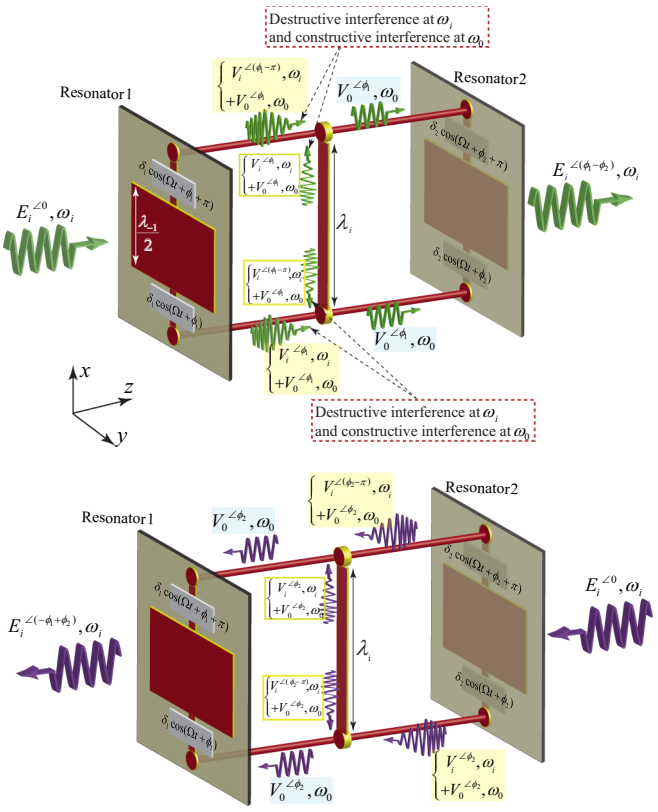

FIG. 5. Forward and backward wave incidences and to the twin time-modulated unit cells.

constructive interference occurs at all even-time harmonics, i.e., $\omega_{n,\text{even}} = \omega_0 + n\Omega$ with n being even, and destructive interference occurs at all odd-time harmonics, i.e., $\omega_{n,\text{odd}} = \omega_0 + n\Omega$ with n being odd. This includes suppression of the dominant odd time harmonic $\omega_i = \omega_0 - \Omega$ ($n = -1$), as well as constructive interference at ω_0 ($n = 0$).

Figure 6(a) shows the structure of a double-fed patch radiator that is suited for efficient radiation with odd excitation. In this figure, the electric field propagation and radiation in a double-fed microstrip patch radiator is sketched, where the left sketch shows efficient radiation of the wave at $\omega_i = \omega_{-1}$ because of odd excitation ($V_i^{\angle 0}$ and $V_i^{\angle \pi}$). The right sketch in Fig. 6(a) demonstrates the transmission-state operation (no radiation) of the structure at ω_0 is ensured due to its even excitation ($V_0^{\angle 0}$ and $V_0^{\angle 0}$).

We suppress all undesired even- and odd-time harmonics, especially $n = -2$, which represents the lower side-band time harmonic of the incident wave. Given the flexibility of the proposed resonance structure in Fig. 5, which is formed by two radiating patch radiators, the proposed twin unit cell inherently operates as a narrow bandpass filter and significantly suppresses all time harmonics that lie outside its passband. Hence, as shown in Fig. 6(b), we design the patch radiators such that $\omega_i = \omega_{-1}$ and $\omega_0 = \omega_i + \Omega$ lie inside the passband of the structure, whereas $\omega_{-2} = \omega_0 - 2\Omega = \omega_i - \Omega$ lies outside the passband (i.e., inside the stopband) of the structure. It should be noted that the modulation frequency Ω is an arbitrary parameter and can be adjusted to guarantee that only the desired time harmonics, here ω_i and ω_0 lie inside the passband of the structure. Thus, all undesired even- and odd-time harmonics are suppressed and safe operation of the structure at ω_i and ω_0 is guaranteed.

Therefore, only two time harmonics ω_i and ω_0 will pass through the first patch element, and the signal at the upper and lower arms of the twin structure reads

$$V(t) = V_{-1}e^{-i([\omega_0-\Omega]t+\phi_1)} + V_0 e^{-i\omega_i t}, \tag{15a}$$

$$V'(t) = V_{-1}e^{-i([\omega_0-\Omega]t+\phi_1+\pi)} + V_0 e^{-i\omega_i t}. \tag{15b}$$

Then, due to the suppression of (short circuit) of the -1 time harmonic (ω_i) by the middle interconnector, the second patch radiator will be fed only at $\omega_0 = \omega_i + \Omega$.

Figures 7(a) and 7(b) elaborate on the suppression of $\omega_i = \omega_{-1}$ by the middle interconnector. Figure 7(a) shows the even-mode operation of the twin unit cells at frequency ω_0, where the two interconnecting horizontal vias are excited in phase, and therefore a virtual open circuit occurs at the middle of the λ long interconnector. This makes the middle interconnector inactive. At the bottom of Fig. 7(a), full-wave simulation results for the power flow for even-mode operation of the twin unit cells at frequency ω_0 are given. It may be seen from this figure that strong power

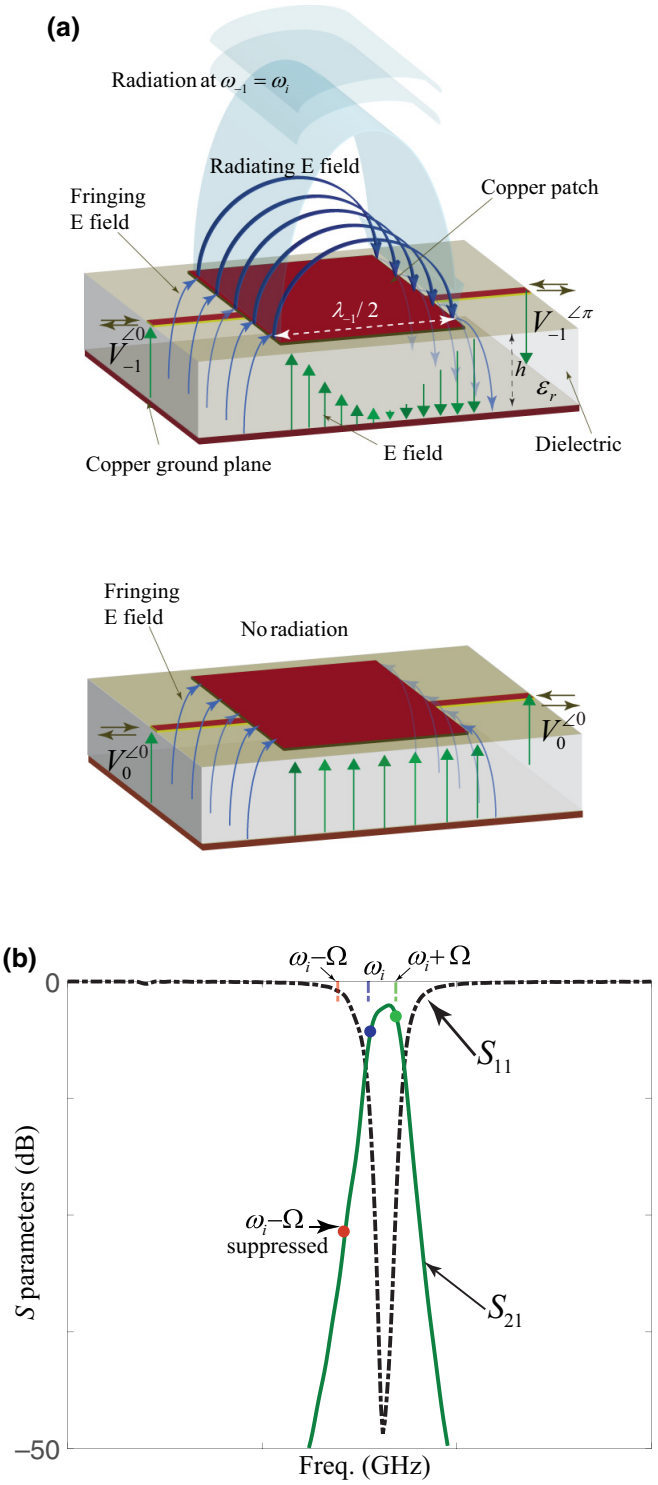

FIG. 6. Electromagnetic wave propagation and radiation in a a double-fed microstrip patch element. (a) Schematic representation of the electric field distribution. (b) Qualitative scattering parameters showing the suppression of $\omega_{-2} = \omega_0 - 2\omega = \omega_i - \omega$.

flows from the left unit cell to the right unit cell through the interconnecting via (at frequency ω_0), where no significant power flows through the middle interconnector due to the

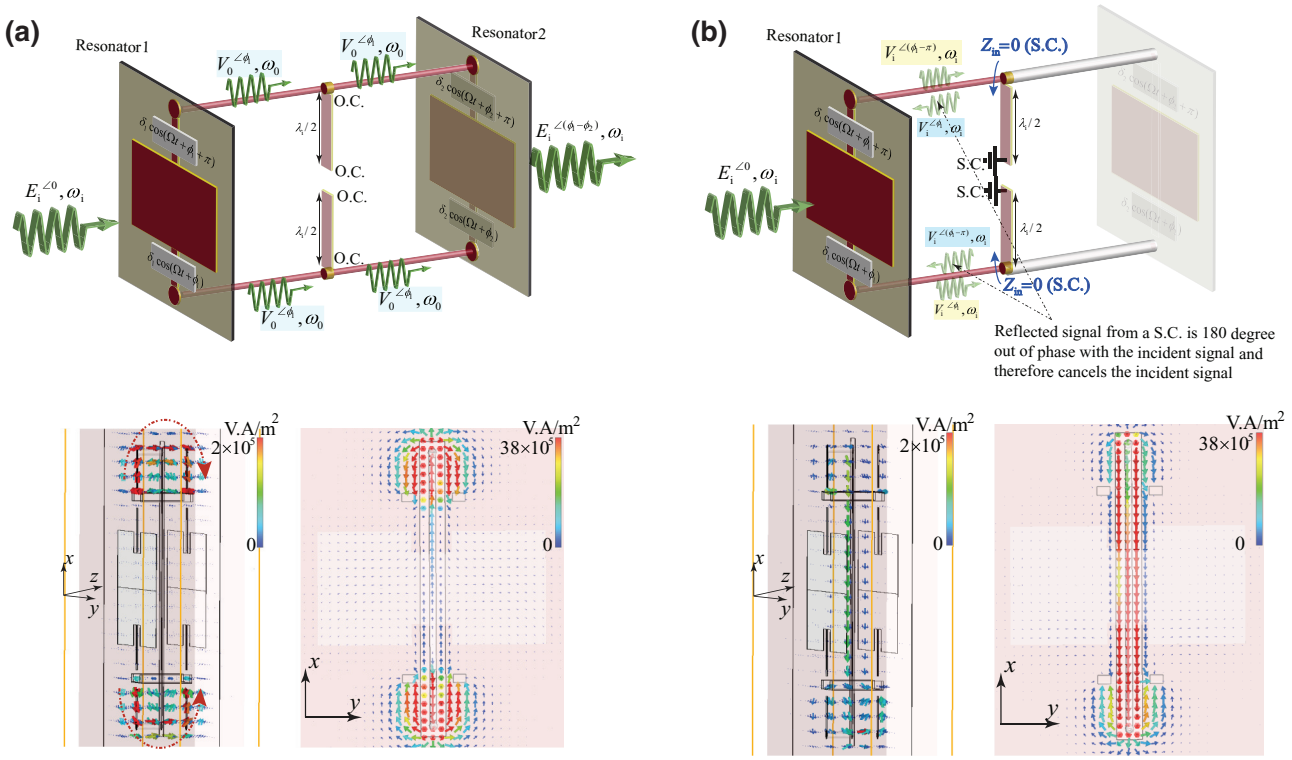

FIG. 7. Schematic representations and full-wave simulation results of the power flow inside the structure for even- and odd-mode operations of the structure at ω_0 and ω_i, respectively. (a) Even-mode operation at ω_0, where the signals at the two horizontal interconnecting vias will reach the second (right) unit cell and no significant power flows through the middle interconnector. (b) Odd-mode operation at ω_i, where weak power flow exists inside the structure and the signals at the two horizontal interconnecting vias will not reach the second (right) unit cell, rather it flows through the middle interconnector.

even excitation of the twin unit cells (0° phase difference between the upper and lower interconnecting vias).

Figure 7(b) shows the odd-mode operation of the twin unit cells at frequency ω_i, where the two interconnecting horizontal vias are excited 180° out of phase, and therefore a virtual short circuit occurs at the middle of the λ long interconnector. This will also make a virtual short circuit at the center of two horizontal arms, hence leading to a total reflection of the incident signals with 180° phase difference with the incident signals. As a result, the incident and reflected signals at the two horizontal interconnecting vias will cancel each other out, and therefore no signal at ω_i would exist at the two horizontal arms of the twin unit cells. At the bottom of Fig. 7(b), full-wave simulation results for the power flow for odd-mode operation of the twin unit cells at frequency ω_i is given. This figure shows that the power flow inside the twin unit cells at frequency ω_i is weak in comparison to the power flow of the even-mode operation, and the power mainly flows through the middle vertical interconnector and does not reach the second (right) unit cell. This is due to the odd excitation of the twin unit cells at the incident frequency ω_i, where 180° phase difference exists between the upper and lower horizontal interconnecting vias.

B. Implementation scenario

Figure 8(a) shows different elements of the twin time-modulated unit cells, providing three major operations, that is, reception of the incoming wave from one side, application of a nonreciprocal phase shift to the wave, and reradiation of the processed phase-shifted wave to the other side of the structure. The unit cell in Fig. 8(a) is formed by twin time-modulated resonators, composed of varactors and lumped elements. Figure 8(b) describes the circuit elements of the twin time-modulated unit cells including the circuit model for the two patch radiators, two 180° phase shifters, two phase shifters with phases ϕ_1 and ϕ_2, respectively, the four varactor diodes D_{var}, four choke inductors L_{chk}, and eight decoupling capacitances C_{cpl}. Two inductances L_{chk} and four capacitances C_{cpl} are employed at each side of the twin unit cells to efficiently prevent the leakage of the incident wave to the modulation path, as well

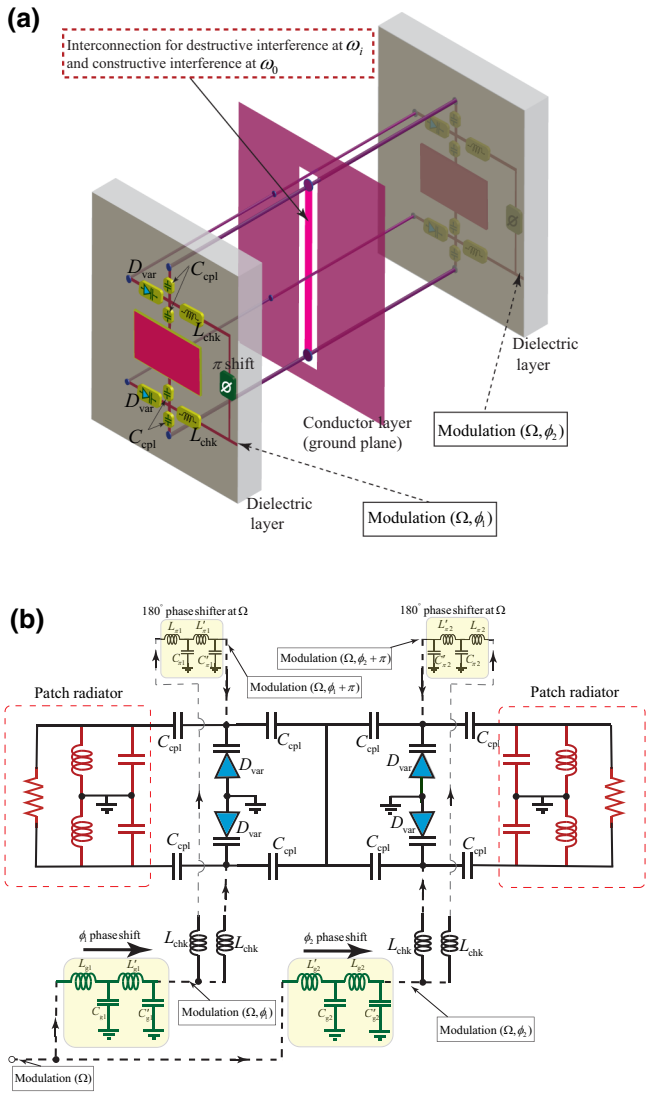

FIG. 8. Unit cell fomed by twin time-modulated resonators. (a) Schematic of the structure. (b) Description of the circuit elements of the twin unit cell including the circuit model for two patch radiators, two 180° phase shifters, two phase shifters with phases ϕ_1 and ϕ_2, respectively, four varactor diodes, four choke inductors, and eight decoupling capacitances.

as decouple the two modulation signals (with 180° phase difference) at the upper and lower side of the unit cell.

Figure 9 depicts a schematic of the complete phase-gradient metasurface comprising 4×4 twin time-modulated unit cells, shown in Fig. 8(a). The modulation signal is fed to the metasurface via a SMA connector. The metasurface includes eight gradient phase shifters (ϕ_1 to ϕ_8), i.e., four phase shifters in each side, providing the required modulation phase shifts for nonreciprocal beam steering. In addition, eight 180° phase shifters (ϕ_π) are utilized for achieving the π phase-shifted version of each gradient phase-shifted modulation signal.

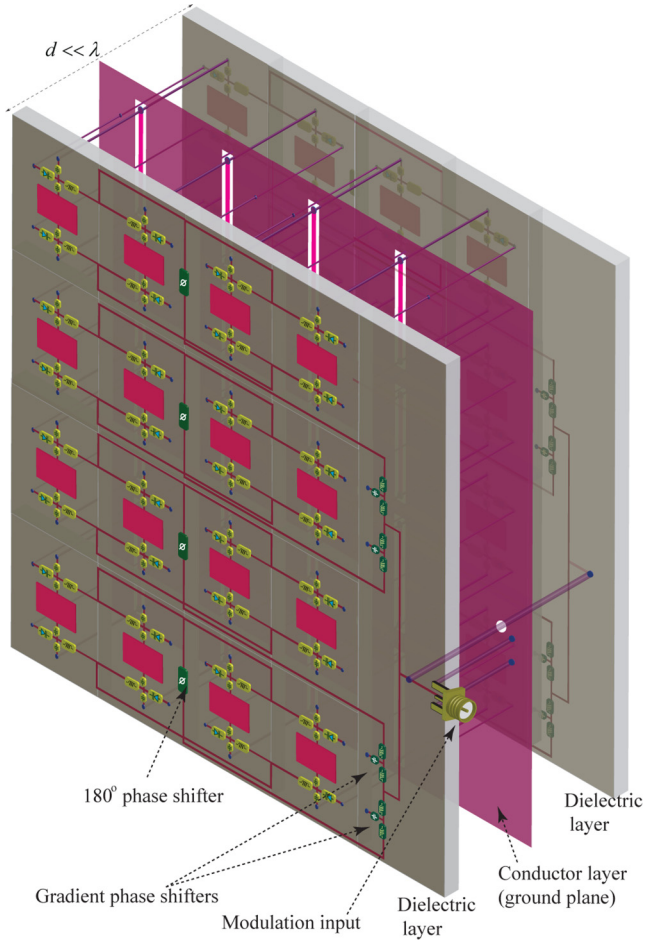

FIG. 9. Architecture of the implemented metasurface composed of 4×4 unit cells.

C. Experimental demonstration

We next experimentally demonstrate the full-duplex nonreciprocal-beam-steering time-modulated transmissive metasurface. Figure 10(a) shows the top view, which includes gradient phase shifters ϕ_1, ϕ_3, ϕ_5, and ϕ_7, and Fig. 10(b) shows the bottom view, which includes gradient phase shifters ϕ_2, ϕ_4, ϕ_6, and ϕ_8. A dc signal is applied to the varactors to achieve the desired average capacitance (average permittivity). A bias tee is used to separate the dc bias and the modulation signal. We employ a total number of 64 SMV1247-079LF varactors (D_{var}) from Skyworks Solutions Inc., 64 inductors of $L_{chk} = 20$ nH, and 128 decoupling capacitances of $C_{cpl} = 5$ pF. The metasurface is fabricated as a three-layer circuit, i.e., three conductor layers and two dielectric layers, made of Rogers RO3210 with 50 mils height ($d = 100$ mils). The incident wave and modulation parameters are set as $\omega_i = 5.28$ GHz, $\Omega = 50$ MHz, and $\omega_0 = \omega_i + \Omega = 5.33$ GHz.

Figure 11(a) depicts a schematic of the measurement setup consisting of two signal generators, a spectrum analyzer and a dc power supply. A photo of the measurement

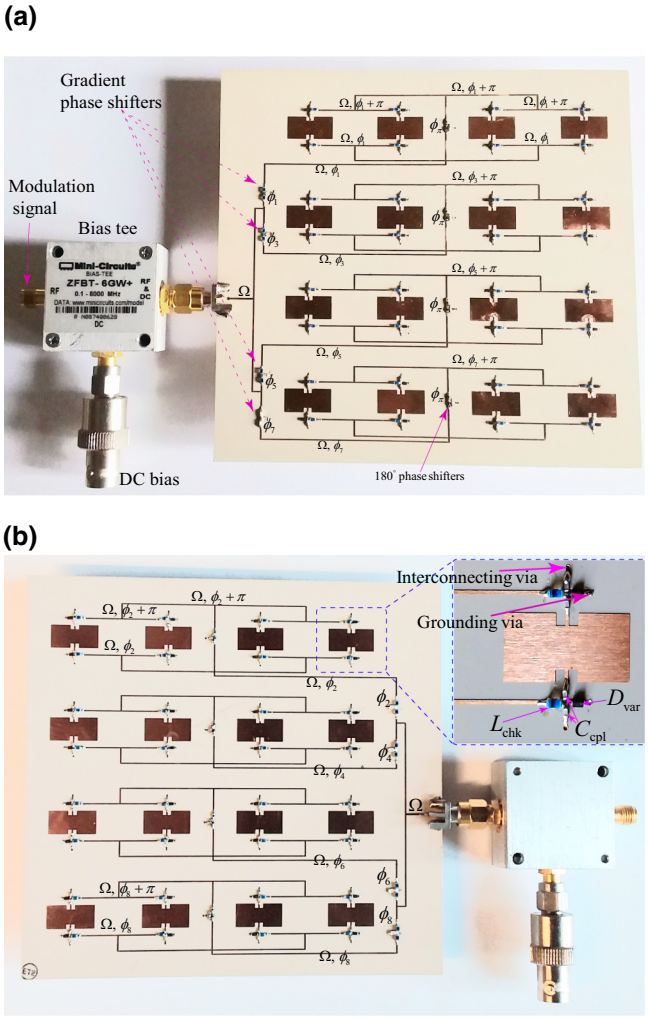

FIG. 10. Experimental demonstration of full-duplex nonreciprocal-beam-steering transmissive phase-gradient metasurface. (a),(b) Top and bottom views of the fabricated prototype, respectively.

setup is shown in Fig. 11(b). Figure 11(c) plots the scattering parameters of the fabricated nonreciprocal radiation beam metasurface. This figure highlights three different frequencies, $\omega_i - \Omega$, ω_i, and $\omega_i + \Omega$. As described in the previous section, two time harmonics ω_i and $\omega_i + \Omega$ lie inside the passband of the structure, whereas $\omega_i - \Omega$ lies in the stopband of the structure and is being suppressed. The scattering parameters are measured using an $E8361C$ Agilent vector network analyzer. For the sake of comparison, we first measure the radiation beam of the unmodulated metasurface, i.e., $\Omega = 0$. Figure 11(d) plots the radiation pattern of the un-modulated metasurface, which is reciprocal, that is, provides identical radiation beams for both transmission and reception states.

Figures 12(a) and 12(b) plot the full-wave simulation results for the nonreciprocal *angle-symmetric* transmission

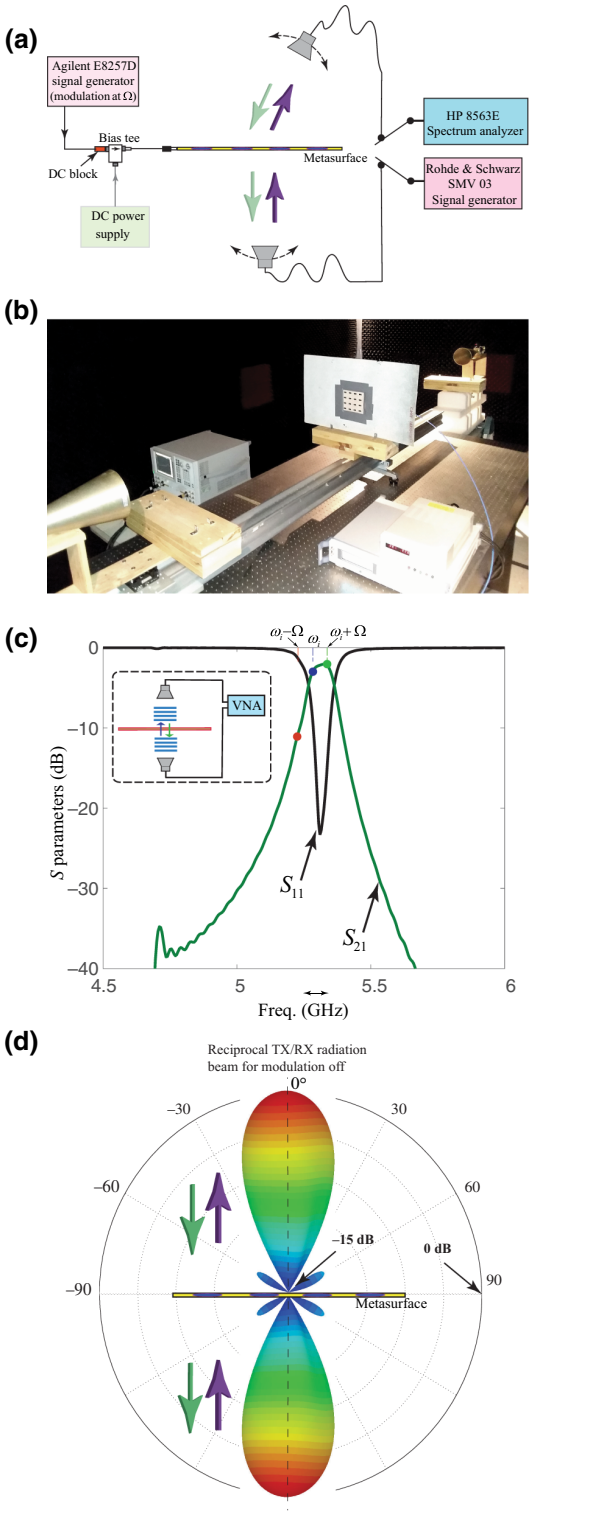

FIG. 11. Experimental demonstration of nonreciprocal radiation beam metasurface. (a) Schematic of the measurement setup consisting of two signal generators, a spectrum analyzer and a dc power supply. (b) Photo of the measurement setup in an anechoic chamber. (c) Experimental results for the scattering parameters of the unmodulated metasurface measured using a vector network analyzer. (d) Simulation results for the reciprocal radiation pattern of the unmodulated metasurface.

and reception radiation patterns of the nonreciprocal radiation beam metasurface for $\theta_{1,TX} = 0$ and $\theta_{1,RX} = 0°$, $\theta_{TX} = -\theta_{RX} = 36°$. Figures 12(c) and 12(d) plot the full-wave simulation results for the nonreciprocal *angle-symmetric* transmission and reception radiation patterns of the nonreciprocal radiation beam metasurface for $\theta_{1,TX} = 0$ and $\theta_{1,RX} = 0°$, $\theta_{TX} = -\theta_{RX} = 52°$. The relation between the angles of reception and transmission and the required nonreciprocal gradient phase shifter for each time-modulated unit cell is governed by Eqs. (2)–(5).

Figure 13 plots the full-wave simulation and experimental results for the nonreciprocal *angle-asymmetric* transmission and reception radiation patterns of the nonreciprocal radiation beam metasurface for $\theta_{1,TX} = \theta_{1,RX} = 9°$, $\theta_{2,TX} = 45°$, and $\theta_{2,RX} = -27°$. In this particular case, the experimental isolation between the transmission and reception radiation patterns at specified transmission radiation angle ($\theta_{2,TX} = 45°$) is about 15.8 dB, and the isolation at specified reception radiation angle ($\theta_{2,RX} = -27°$) is about 10.4 dB. To achieve higher isolation levels, one may change the modulation parameters or use a more directive metasurface by increasing the number of twin unit cells. Figure 13(c) plots the full-wave simulation results demonstrating the full-duplex angle-symmetric or asymmetric beam-steering functionality of the time-modulated gradient transmissive metasurface. In this figure, four different gradient profiles are considered, that is, A, B, C, and D.

Figures 14(b) and 14(a) plot the experimental results for the spectra of the transmitted and received waves at different angles, respectively, with the nonreciprocal beam presented in the bottom of Fig. 13(b), i.e., $\theta_{TX,2} = 45°$,

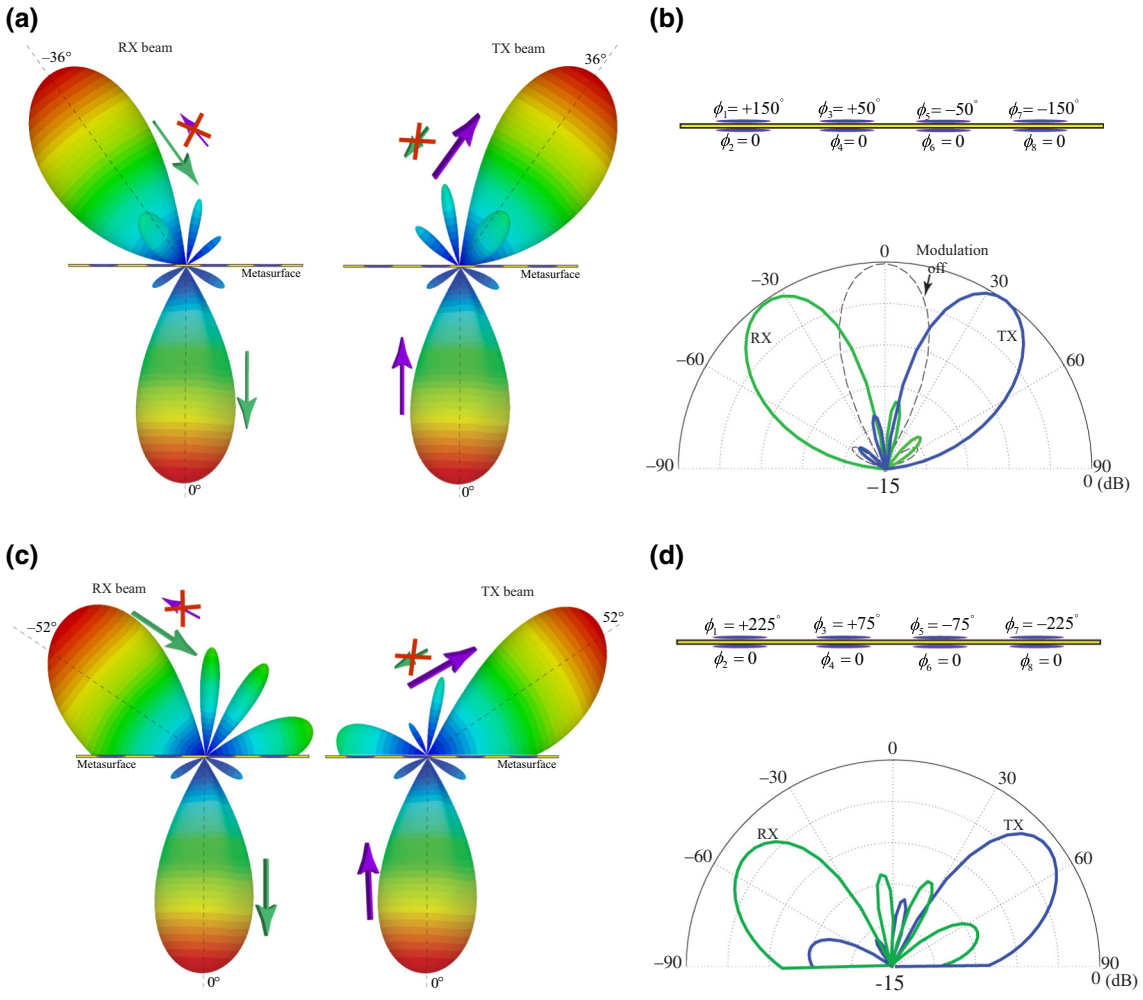

FIG. 12. Full-wave simulation results for angle-symmetric transmission and reception radiation patterns of the nonreciprocal-beam metasurfcae. (a),(b) Simulation results for the normalized radiation beam at the two sides of the metasurface for reception and transmission for $\theta_{TX} = -\theta_{RX} = 36°$. (c),(d) Simulation results for the normalized radiation beam at the two sides of the metasurface for reception and transmission for $\theta_{TX} = -\theta_{RX} = 52°$.

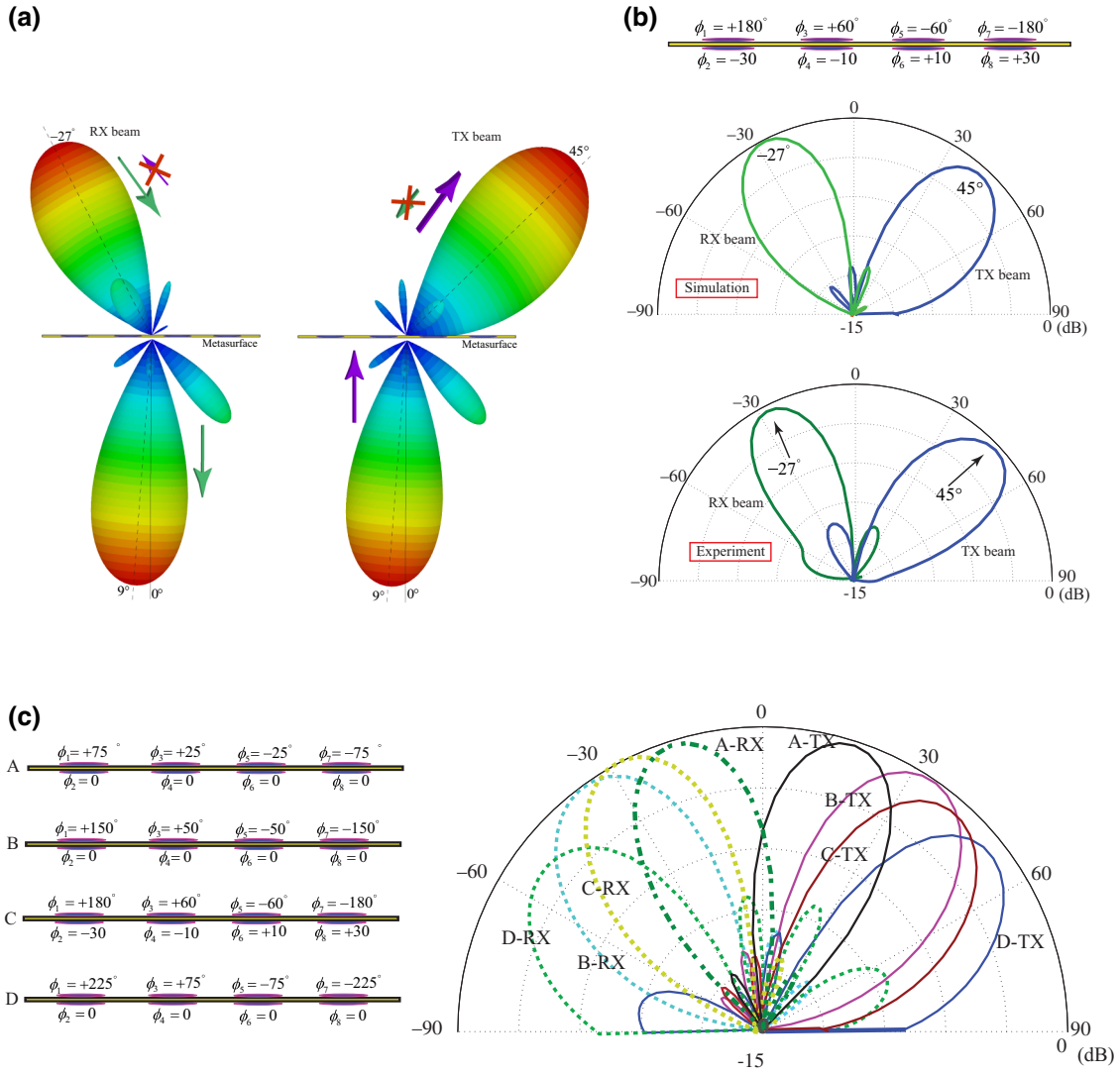

FIG. 13. Full-wave simulation and experimental results. (a) Angle-asymmetric transmission and reception radiation patterns of the nonreciprocal-beam metasurface. Simulation results show the normalized radiation beam at the two sides of the metasurface for (left) reception and (right) transmission, corresponding to $\theta_{TX,2} = 45°$, $\theta_{RX,2} = -27°$, $\theta_{TX,1} = \theta_{RX,1} = 9°$. (b) Results for the TX and RX normalized radiation beams in comparison with reciprocal normalized radiation beam for modulation off. (Top) Simulation, and (bottom) experimental results. (c) Full-duplex angle-symmetric or asymmetric beam steering.

$\theta_{RX,2} = -27°$, $\theta_{TX,1} = \theta_{RX,1} = 9°$. These figures show that the unwanted time harmonics are significantly suppressed.

V. DISCUSSION

(a) The main concept of this paper is the realization of a transmissive metasurface, which is capable of *nonreciprocal beam* generation. Such a metasurface gives the opportunity to realize full-duplex transmission where simultaneous transmission and reception of waves are performed but at different angles. This is quite distinct from other proposed nonreciprocal (isolator) metasurfaces [1,2,42,44,62]. Such a functionality, i.e., a nonreciprocal beam, is very practical and different than other recently proposed "nonreciprocal" (isolator) metasurfaces in which the structure allows the transmission of the wave only in one direction, whereas the wave coming from the opposite direction is totally reflected or absorbed.

(b) Furthermore, most of the recently proposed nonreciprocal metasurfaces operate only in the *reflective* state [1,42,44,62], and therefore are less practical. In our paper, we propose a mechanism to achieve *nonreciprocal beam* operation in the transmission state, so that the structure can be used as a radome for antennas.

(c) We stress that all previously proposed nonreciprocal time-modulated metasurfaces suffer from an unwanted frequency change in the spectrum of the incident wave, so that the transmitted wave acquires a different

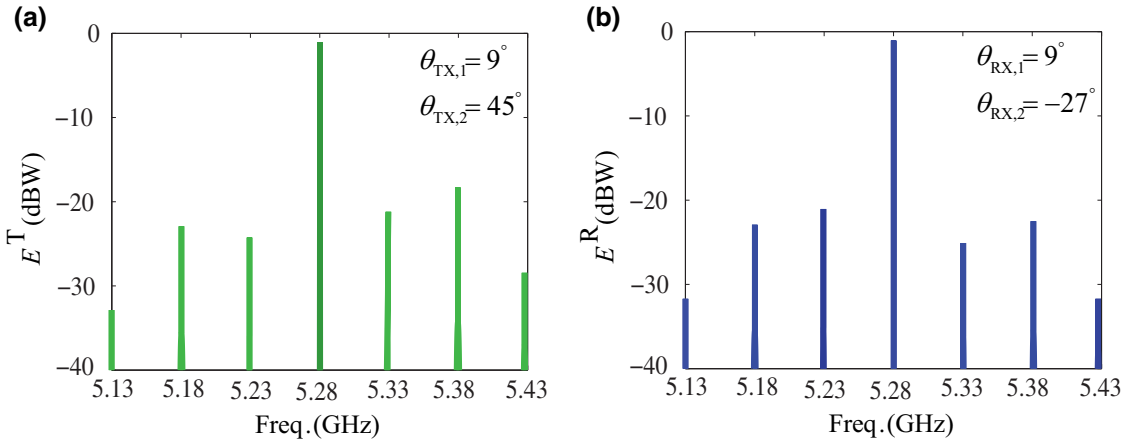

FIG. 14. Experimental results for the spectra of the transmitted and received waves, associated with the nonreciprocal beam in the bottom of Fig. 13(b), i.e., $\theta_{TX,2} = 45°$, $\theta_{RX,2} = -27°$, $\theta_{TX,1} = \theta_{RX,1} = 9°$. (a) Transmitted wave. (b) Received wave.

frequency than the incident wave. However, in our proposed nonreciprocal-beam metasurface, the incident and transmitted waves share the same frequency. Hence, the proposed metasurface is more practical.

(d) In terms of the physics, we show that one can leverage the unique properties of frequency-phase transitions in time-modulated unit cells to realize a radiating nonreciprocal phase shifter, whereas all the unwanted time harmonics are suppressed in an elegant manner.

It should be noted that there is no inherent limit to the bandwidth enhancement of the proposed structure. The frequency bandwidth of the proposed unit cells can be easily enhanced up to 100%, simply by using engineering approaches for the bandwidth enhancement of patch elements [63,64]. We stress that in the proposed twin-unit-cell topology, the suppression of unwanted harmonics is not related to the narrowband operation of the structure. One may use broadband patch elements and at the same time increase the modulation frequency so that the entire architecture operates in the same way, that is, only two desired time harmonics fall inside the passband of the structure and all other undesired harmonics fall inside the stopband. In other words, our proposed architecture is very flexible and can be used for different scenarios.

(e) To achieve a strong isolation between the transmission and reception beams in practice, a fairly high-power modulation signal is required (e.g., modulation power stronger than 10 dBm). However, part of the modulation power couples to the incident wave and results in a very low insertion loss, or a transmission gain depending on the modulation parameters [27]. The overall insertion loss of the metasurface depends on the microstrip patch radiators, resistance of the varactors, and modulation parameters.

(f) Varactor diodes can provide gain without introducing significant noise. However, there exist several potential sources of noise, i.e., thermal noise of the series resistance of varactor, shot noise of the forward current, shot noise of the reverse current, ionization noise, and reverse-breakdown noise [65]. The noise analysis and noise figure calculation in varactor-based circuits is presented in Ref. [65]. It has been shown experimentally that varactor-based amplifiers and circuits introduce much lower noise in comparison to other techniques [66–68]. In the lab experiment, we achieve a noise figure of lower than 2.15 dB for both receive and transmit states. The noise figure is determined by subtracting the signal-to-noise ratios of the incident and transmitted signals.

(g) Recently, nonreciprocal [1,3,17,38,42,69] and asymmetric [4,70–75] wave transmission, reflection, diffraction, and absorption have attracted a surge of scientific interest. However, there exist substantial difference between the nonreciprocity and asymmetry in electromagnetic structures as follows [58]. Asymmetric structures are linear and time invariant, as they are restricted to the Lorentz reciprocity theorem and cannot be used as *wave isolators or for nonreciprocal-beam operation*. In general, all time-invariant linear systems, represented by symmetric electric permittivity tensors and symmetric magnetic permeability tensors, are governed by the Lorentz reciprocity theorem. Thus, they are reciprocal as their scattering matrices are symmetric even if the electric permittivity tensor or the magnetic permeability tensor are complex.A comprehensive explanation of the difference between the excitation and response for distinguishing between the symmetry and reciprocity of electromagnetic structures is presented in Ref. [58]. As shown in Ref. [58], the main difference in the reciprocity and symmetry experiments is in the *backward excitation*. For a symmetry experiment, the backward excitation (input) wave should be the spatial inversion of the forward excitation (input) wave. Then, the output of the backward problem should be exactly the spatial inversion of the output of the forward problem. Otherwise,

the system is asymmetric. By contrast, for the reciprocity experiment, the backward excitation (input) wave should be the *spatial inversion of the time-reversed* forward problem, i.e., the applied excitation wave (input) of the backward problem must be the spatial inversion of the *output* of the forward problem. Then, the output of the backward problem should be exactly the spatial inversion of the *input* of the forward problem. Otherwise, the system is nonreciprocal.

VI. CONCLUSION

We present a theoretical and experimental strategy for the realization of full-duplex nonreciprocal-beam-steering transmissive metasurfaces. Such a strategy takes advantage of the unique and peculiar properties of asymmetric frequency-phase transitions in twin time-modulated unit cells. The proposed twin-unit-cell architecture leverages the extraordinary operation of periodic double-fed time-modulated patch antennas, and their associated peculiar frequency-phase transitions. The metasurfaces are composed of an array of twin time-modulated unit cells, each of which is fed by a specified modulation phase, such that a phase-gradient modulation is applied to the twin unit cells. As a result of such a gradient modulation phase, a nonreciprocal-phase-gradient metasurface is realized and therefore, the incoming (received) and outgoing (transmitted) waves are radiated at different radiation angles. We show that the proposed twin time-modulated unit cells inherently prohibit the excitation of undesired time harmonics. This results in a high conversion efficiency, i.e., less than 1-dB insertion loss, which is of paramount importance for practical applications such as, for instance, point-to-point full-duplex communications. It should be noted that the low insertion loss of the metasurface is supported by the injection of the energy from the time modulation to the incident wave. The proposed metasurface is expected to find applications in point-to-point full-duplex wireless communication systems that require highly directive radiation beams, offering the possibility of different half-power beamwidths, for the transmission and reception states. This includes satellite communications and cellular communication systems.

[1] Yakir Hadad, Dimitrios L. Sounas, and Andrea Alù, Space-time gradient metasurfaces, Phys. Rev. B **92**, 100304 (2015).

[2] Sajjad Taravati, Bakhtiar A. Khan, Shulabh Gupta, Karim Achouri, and Christophe Caloz, Nonreciprocal nongyrotropic magnetless metasurface, IEEE Trans. Antennas Propagat. **65**, 3589 (2017).

[3] Yu Shi and Shanhui Fan, Dynamic non-reciprocal metasurfaces with arbitrary phase reconfigurability based on photonic transition in meta-atoms, Appl. Phys. Lett. **108**, 021110 (2016).

[4] Xuchen Wang, Ana Díaz-Rubio, Viktar S. Asadchy, Grigorii Ptitcyn, Andrey A. Generalov, Juha Ala-Laurinaho, and Sergei A. Tretyakov, Extreme Asymmetry in Metasurfaces via Evanescent Fields Engineering: Angular-Asymmetric Absorption, Phys. Rev. Lett. **121**, 256802 (2018).

[5] Zhanni Wu and Anthony Grbic, Serrodyne frequency translation using time-modulated metasurfaces, arXiv:1905.06792 (2019).

[6] Jia Wei Zang, Xi Tang Wang, Alejandro Alvarez-Melcon, and Juan Sebastian Gomez-Diaz, Nonreciprocal Yagi-Uda filtering antennas, arXiv:1906.06418 (2019).

[7] Sajjad Taravati and Ahmed A. Kishk, Advanced wave engineering via obliquely illuminated space-time-modulated slab, IEEE Trans. Antennas Propagat. **67**, 270 (2019).

[8] Grigorii A. Ptitcyn, Mohammad Sajjad Mirmoosa, and Sergei A. Tretyakov, Time-modulated meta-atoms, Phys. Rev. Res. **1**, 023014 (2019).

[9] D. R. Smith, J. B. Pendry, and M. C. K. Wiltshire, Metamaterials and negative refractive index, Science **305**, 788 (2004).

[10] Bogdan-Ioan Popa and Steven A. Cummer, Nonreciprocal active metamaterials, Phys. Rev. B **85**, 205101 (2012).

[11] T. Kodera, D. L. Sounas, and C. Caloz, Magnetless nonreciprocal metamaterial (MNM) technology: Application to microwave components, IEEE Trans. Microw. Theory Techn. **61**, 1030 (2013).

[12] Yarden Mazor and Ben Z. Steinberg, Metawaves: Sector-Way Nonreciprocal Metasurfaces, Phys. Rev. Lett. **112**, 153901 (2014).

[13] Sajjad Taravati and Ahmed A. Kishk, Space-time modulation: Principles and applications, IEEE Microw. Mag. **21**, 30 (2020).

[14] Edward S. Cassedy, Waves guided by a boundary with time-space periodic modulation, IET **112**, 269 (1965).

[15] Edwards S. Cassedy, Dispersion relations in time-space periodic media: Part II-unstable interactions, Proc. IEEE **55**, 1154 (1967).

[16] Sajjad Taravati, Ph.D. thesis, School École Polytechnique de Montréal, 2017.

[17] Sajjad Taravati, Giant Linear Nonreciprocity, Zero Reflection, and Zero Band gap in Equilibrated Space-Time-Varying Media, Phys. Rev. Appl. **9**, 064012 (2018).

[18] Sandeep Inampudi, Mohammad Mahdi Salary, Samad Jafar-Zanjani, and Hossein Mosallaei, Rigorous space-time coupled-wave analysis for patterned surfaces with temporal permittivity modulation, Opt. Mater. Express **9**, 162 (2019).

[19] Sameh Y. Elnaggar and Gregory N. Milford, Generalized space-time periodic circuits for arbitrary structures, arXiv:1901.08698 (2019).

[20] Sajjad Taravati and Ahmed A. Kishk, Dynamic modulation yields one-way beam splitting, Phys. Rev. B **99**, 075101 (2019).

[21] Neng Wang, Zhao-Qing Zhang, and C. T. Chan, Photonic Floquet media with a complex time-periodic permittivity, Phys. Rev. B **98**, 085142 (2018).

[22] Jorge R. Zurita-Sánchez, P. Halevi, and Juan C. Cervantes-Gonzalez, Reflection and transmission of a wave incident on a slab with a time-periodic dielectric function, Phys. Rev. A **79**, 053821 (2009).

[23] Juan Sabino Martínez-Romero and P. Halevi, Parametric resonances in a temporal photonic crystal slab, Phys. Rev. A **98**, 053852 (2018).
[24] Mohammad Mahdi Salary, Samad Jafar-Zanjani, and Hossein Mosallaei, Time-varying metamaterials based on graphene-wrapped microwires: Modeling and potential applications, Phys. Rev. B **97**, 115421 (2018).
[25] Mohammad Sajjad Mirmoosa, Grigorii Ptitcyn, Viktar S. Asadchy, and Sergei A. Tretyakov, Time-Varying Reactive Elements for Extreme Accumulation of Electromagnetic Energy, Phys. Rev. Appl. **11**, 014024 (2019).
[26] Zongfu Yu and Shanhui Fan, Integrated nonmagnetic optical isolators based on photonic transitions, IEEE J. Sel. Top. Quantum Electron. **16**, 459 (2009).
[27] Junfei Li, Chen Shen, Xiaohui Zhu, Yangbo Xie, and Steven A. Cummer, Nonreciprocal sound propagation in space-time modulated media, Phys. Rev. B **99**, 144311 (2019).
[28] Mourad Oudich, Yuanchen Deng, Molei Tao, and Yun Jing, Space-time phononic crystals with anomalous topological edge states, arXiv:1904.02711 (2019).
[29] Diego Correas Serrano, Andrea Alù, and Juan Sebastian Gomez-Diaz, Magnetic-free nonreciprocal photonic platform based on time-modulated graphene capacitors, Phys. Rev. B **98**, 165428 (2018).
[30] Mingkai Liu, David A. Powell, Yair Zarate, and Ilya V. Shadrivov, Huygens' Metadevices for Parametric Waves, Phys. Rev. X **8**, 031077 (2018).
[31] Zhi-Xia Du, Aobo Li, Xiu Yin Zhang, and Daniel F. Sievenpiper, A simulation technique for radiation properties of time-varying media based on frequency-domain solvers, IEEE Access **7**, 112375 (2019).
[32] John L. Wentz, A nonreciprocal electrooptic device, Proc. IEEE **54**, 97 (1966).
[33] Hugo Lira, Zongfu Yu, Shanhui Fan, and Michal Lipson, Electrically Driven Nonreciprocity Induced by Interband Photonic Transition on a Silicon Chip, Phys. Rev. Lett. **109**, 033901 (2012).
[34] Kejie Fang, Zongfu Yu, and Shanhui Fan, Photonic Aharonov-Bohm Effect Based on Dynamic Modulation, Phys. Rev. Lett. **108**, 153901 (2012).
[35] Kejie Fang, Zongfu Yu, and Shanhui Fan, Experimental demonstration of a photonic aharonov-bohm effect at radio frequencies, Phys. Rev. B **87**, 060301 (2013).
[36] Shihan Qin, Qiang Xu, and Yuanxun Ethan Wang, Nonreciprocal components with distributedly modulated capacitors, IEEE Trans. Microw. Theory Techn. **62**, 2260 (2014).
[37] Mehdi B. Zanjani, Arthur R. Davoyan, Ahmed M. Mahmoud, Nader Engheta, and Jennifer R. Lukes, One-way phonon isolation in acoustic waveguides, Appl. Phys. Lett. **104**, 081905 (2014).
[38] Sajjad Taravati, Nima Chamanara, and Christophe Caloz, Nonreciprocal electromagnetic scattering from a periodically space-time modulated slab and application to a quasisonic isolator, Phys. Rev. B **96**, 165144 (2017).
[39] Sajjad Taravati, Self-biased broadband magnet-free linear isolator based on one-way space-time coherency, Phys. Rev. B **96**, 235150 (2017).
[40] Nicholas Aaron Estep, Dimitrios L. Sounas, and Andrea Alù, Magnetless microwave circulators based on spatiotemporally modulated rings of coupled resonators, IEEE Trans. Microw. Theory Techn. **64**, 502 (2016).
[41] Tolga Dinc, Aravind Nagulu, and Harish Krishnaswamy, A millimeter-wave non-magnetic passive soi cmos circulator based on spatio-temporal conductivity modulation, IEEE J. Solid-State Circuits **52**, 3276 (2017).
[42] Yu Shi, Seunghoon Han, and Shanhui Fan, Optical circulation and isolation based on indirect photonic transitions of guided resonance modes, ACS Photonics **4**, 1639 (2017).
[43] Mohammad Mahdi Salary, Samad Jafar-Zanjani, and Hossein Mosallaei, Electrically tunable harmonics in time-modulated metasurfaces for wavefront engineering, New J. Phys. **20**, 123023 (2018).
[44] Joachim Werner Zang, Diego Correas-Serrano, J. T. S. Do, Xiaoguang Liu, Alejandro Alvarez-Melcon, and Juan Sebastian Gomez-Diaz, Nonreciprocal Wavefront Engineering with Time-Modulated Gradient Metasurfaces, Phys. Rev. Appl. **11**, 054054 (2019).
[45] Sajjad Taravati, Aperiodic space-time modulation for pure frequency mixing, Phys. Rev. B **97**, 115131 (2018).
[46] Sajjad Taravati and Christophe Caloz, Mixer-duplexer-antenna leaky-wave system based on periodic space-time modulation, IEEE Trans. Antennas Propagat. **65**, 442 (2017).
[47] Hershel Shanks, A new technique for electronic scanning, IEEE Trans. Antennas Propag. **9**, 162 (1961).
[48] Sajjad Taravati and Christophe Caloz, in *IEEE AP-S Int. Antennas Propagat. (APS)* (IEEE, Vancouver, Canada, 2015).
[49] Yakir Hadad, Jason Christopher Soric, and Andrea Alù, Breaking temporal symmetries for emission and absorption, Proc. Natl. Acad. Sci. **113**, 3471 (2016).
[50] Davide Ramaccia, Dimitrios L. Sounas, Andrea Alù, Filiberto Bilotti, and Alessandro Toscano, Nonreciprocity in antenna radiation induced by space-time varying metamaterial cloaks, IEEE Antennas Wirel. Propagat. Lett. **17**, 1968 (2018).
[51] Mohammad Mahdi Salary, Samad Jafar-Zanjani, and Hossein Mosallaei, Nonreciprocal optical links based on time-modulated nanoantenna arrays: Full-duplex communication, Phys. Rev. B **99**, 045416 (2019).
[52] Sajjad Taravati and Ahmed A. Kishk, in *2018 18th International Symposium on Antenna Technology and Applied Electromagnetics (ANTEM)* (IEEE, Waterloo, Canada, 2018).
[53] Sajjad Taravati and George V. Eleftheriades, in *2019 13th International Congress on Artificial Materials for Novel Wave Phenomena (Metamaterials)* (IEEE, Rome, Italy, 2019).
[54] Alejandro Alvarez-Melcon, Xinjun Wu, Jun-wei Zang, Xiaoguang Liu, and Juan Sebastian Gomez-Diaz, Coupling matrix representation of nonreciprocal filters based on time modulated resonators, arXiv:1905.08340 (2019).
[55] Xiaohu Wu, Xiaoguang Liu, Mark D. Hickle, Dimitrios Peroulis, Juan Sebastián Gómez-Díaz, and Alejandro

Álvarez Melcón, Isolating bandpass filters using time-modulated resonators, IEEE Trans. Microw. Theory Techn. **67**, 2331 (2019).

[56] Amir Shlivinski and Yakir Hadad, Beyond the Bode-Fano Bound: Wideband Impedance Matching for Short Pulses Using Temporal Switching of Transmission-Line Parameters, Phys. Rev. Lett. **121**, 204301 (2018).

[57] Paloma Arroyo Huidobro, Emanuele Galiffi, Sebastien Guenneau, Richard V. Craster, and John B. Pendry, Fresnel drag in space-time modulated metamaterials, arXiv:1908.05883 (2019).

[58] Sajjad Taravati and George V. Eleftheriades, Generalized Space-Time Periodic Diffraction Gratings: Theory and Applications, Phys. Rev. Appl. **12**, 024026 (2019).

[59] Sajjad Taravati and George V. Eleftheriades, Space-time medium functions as a perfect antenna-mixer-amplifier transceiver, arXiv:2005.00807 (2020).

[60] Joshua N. Winn, Shanhui Fan, John D. Joannopoulos, and Erich P. Ippen, Interband transitions in photonic crystals, Phys. Rev. B **59**, 1551 (1999).

[61] Po Dong, Stefan F. Preble, and Jacob T. Robinson, Sasikanth Manipatruni, and Michal Lipson: Inducing Photonic Transitions between Discrete Modes in a Silicon Optical Microcavity, Phys. Rev. Lett. **100**, 033904 (2008).

[62] Xuexue Guo, Yimin Ding, Yao Duan, and Xingjie Ni, Nonreciprocal metasurface with space-time phase modulation, Light Sci. Appl. **8**, 1 (2019).

[63] Alireza Moradi and Tharek Abdul Rahman, Broadband modified rectangular microstrip patch antenna using stepped cut at four corners method, Prog. Electromag. Res. **137**, 599 (2013).

[64] Amer Bzeih, Soubhi Abou Chahine, Karim Y. Kabalan, Ali El-Hajj, and Ali Chehab, An improved broadband e patch microstrip antenna for wireless communications, Radio Sci. **42**, 1 (2007).

[65] F. J. Hyde, Varactor-diode parametric amplifiers, IET **111**, 1080 (1964).

[66] S. Kita and K. Tahara, Low-noise 11-gc parametric amplifier using refrigerated silver-bonded germanium diode, Proc. IEEE **51**, 618 (1963).

[67] Wooram Lee and Ehsan Afshari, Low-noise parametric resonant amplifier, IEEE Trans. Circuits Syst. I: Regular Papers **58**, 479 (2011).

[68] Yun Shi Li, Xiao Peng Yu, and Zheng Hao Lu, Nonreciprocal time-varying transmission line with carrier boosting technique for low-noise rf front ends, IEEE Microw. Wireless Compon. Lett. **28**, 1011 (2018).

[69] Dynamic Nonreciprocity in Loss-Compensated Piezophononic Media, Phys. Rev. Appl. **9**, 034033 (2018).

[70] V. A. Fedotov, P. L. Mladyonov, S. L. Prosvirnin, A. V. Rogacheva, Y. Chen, and N. I. Zheludev, Asymmetric Propagation of Electromagnetic Waves through a Planar Chiral Structure, Phys. Rev. Lett. **97**, 167401 (2006).

[71] R. Singh, E. Plum, C. Menzel, C. Rockstuhl, A. K. Azad, R. A. Cheville, F. Lederer, W. Zhang, and N. I. Zheludev, Terahertz metamaterial with asymmetric transmission, Phys. Rev. B **80**, 153104 (2009).

[72] Liang Feng, Maurice Ayache, Jingqing Huang, Ye-Long Xu, Ming-Hui Lu, Yan-Feng Chen, Yeshaiahu Fainman, and Axel Scherer, Nonreciprocal light propagation in a silicon photonic circuit, Science **333**, 729 (2011).

[73] Semih Cakmakyapan, Andriy E. Serebryannikov, Humeyra Caglayan, and Ekmel Ozbay, Spoof-plasmon relevant one-way collimation and multiplexing at beaming from a slit in metallic grating, Opt. Express **20**, 26636 (2012).

[74] Shanhui Fan, Roel Baets, Alexander Petrov, Zongfu Yu, John D. Joannopoulos, Wolfgang Freude, Andrea Melloni, Miloš Popović, Mathias Vanwolleghem, Dirk Jalas, *et al.*, Comment on "nonreciprocal light propagation in a silicon photonic circuit", Science **335**, 38 (2012).

[75] Mohsin Habib, Andriy E. Serebryannikov, Humeyra Caglayan, Guy A. E. Vandenbosch, and Ekmel Ozbay, Connection of collimation, asymmetric beaming, and independent transmission-reflection processes in concentric-groove gratings supporting spoof surface plasmons, Plasmonics **14**, 721 (2019).